THERMAL MODELING AND MEASUREMENTS OF AN ENGINEERING MODEL HALL THRUSTER

A. Warshavsky (avrahamw@rafael.co.il)
Manor Division, Rafael, Haifa 31021, Israel
I. Zur (israelz@rafael.co.il)
Mechanical CAD Division, Rafael, Haifa 31021, Israel
J. Ashkenazy (joseph@soreq.gov.il) and **G. Appelbaum**
Propulsion Physics Laboratory, Soreq NRC, Yavne 81800, Israel

Abstract

Body temperatures of an engineering model Hall thruster were measured with embedded thermocouples at three power levels, while channel surface temperatures were observed with a thermal imaging camera. Doubling the thruster power from 306 to 600 Watts resulted in a modest increase of less than 14% in the steady-state temperatures, with the time to steady-state being longer than an hour. Steady-state measurement results were used to check and calibrate a 3D finite-element thermal model of the thruster, which takes into account both conduction and radiation. A good convergence of measured and calculated temperatures was obtained at the three power levels, from which an insight about the heat loads on different thruster parts could be gained.

1. Introduction

The large specific impulse, high efficiency, and compactness of the Hall thruster represent a combination of properties that make this type of thruster attractive for use onboard small spacecraft in large Δv missions. Nevertheless, due to the characteristically low thrust, the accomplishment of a typical mission may require overall thousands of hours of thruster operation for which it has to operate without malfunction or significant degradation. An important element in the development of a flight model thruster able to endure such prolonged operating time is the knowledge of the temperatures developed during operation in different parts of the thruster, which may affect the selection of proper materials and production methods.

As part of a joint effort to develop flight qualified Hall thrusters, an engineering model (EM) thruster was constructed at Rafael Space Propulsion Department in collaboration with Soreq. The design of the thruster, intended to operate in the 200-800 Watts power range, is based on laboratory model thrusters developed and thoroughly investigated at Soreq [1]. The EM thruster is a stage in a development process in which technological improvements, including mass reduction techniques, were introduced into its design, and its reliable operation over long periods is being investigated in order to bring it to a flight configuration. The tests of the EM thruster are conducted at the Soreq test facility. The flight derivatives of the EM thruster are planned to be used onboard light spacecraft, in the 100-200 kg mass range, which are being considered for future missions, such as the one described in [2].

The issue of thruster temperature distribution was addressed both experimentally and theoretically. Thruster body temperatures were measured with six embedded thermocouples at three power levels, while channel surface temperatures were observed with a thermal imaging camera. These experiments are described in

section 2. Time-dependent temperature profiles were sampled from thruster turn-on to thermal steady-state and during the cooling phase after turn-off. It was observed that doubling the thruster power from 306 to 600 Watts leads to a modest increase in the steady-state body temperatures of less than 14%. It takes more than an hour for the thruster to approach a thermal steady-state, the time being longer for lower input power.
The analysis in section 3 provides rough estimates for the power dissipated in the thruster internal surfaces, based on results obtained earlier at Soreq [1] and at other laboratories. The estimates served as first iteration input to a 3D finite-element thermal model of the thruster. The thruster thermal model, described in section 4, was constructed using the COSMOS/Works software. The software package was augmented by an iterative process that enabled to take account of the mutual radiation between adjacent surfaces in a self-consistent way. Steady-state measurement results were used to check and calibrate the thruster thermal model. A good convergence of measured and calculated temperatures was obtained at the three power levels, from which an insight about the heat loads on different thruster parts could be gained.

2. Thruster thermal measurements

Operational tests of the EM thruster were performed at the Soreq electric propulsion laboratory in a 3.1×1.2 meter vacuum chamber equipped with two APD-22 cryopumps. The chamber ambient pressure during thruster operation was $2\text{-}4\cdot10^{-5}$ Torr. Thruster body temperatures were measured using six embedded ungrounded metal-sheathed K-type thermocouples. The schematic drawing of the thruster in Fig. 1 shows their locations: T1 - below the central coil, T2 – behind the internal pole, T3 – at the back of the magnetic circuit, T4 – on the holder of the ceramic channel, T5 – on the holder of the cathode, and T6 – on the gas supply pipe to the anode.

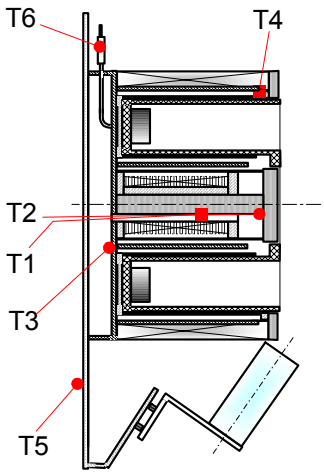

Figure 1: Schematic drawing of the thruster showing the locations of the embedded thermocouples, T1-T6.

Temperature measurements during thruster operation at a discharge voltage of 300V were taken at three power levels: 306 Watts, 430 Watts, and 600 Watts. In addition, temperatures were measured also in two

cases in which the thruster coils carried current but the thruster was not operated. The measured thrust, specific impulse and efficiency at the three power levels are presented in Table 1.

Table 1: Measured thruster performance at the three power levels. The discharge voltage was 300V.

Power (Watts)	Anode Flow (mg/s)	Thrust (mN)	Isp* (sec)	Eff.* (%)
306	1.15	16.5	1465	39
430	1.56	24	1570	43
600	2.11	35	1690	48.5

* Cathode mass flow is not included.

In all three cases, the thruster was at ambient chamber temperature just before turn-on. In each case, the thruster was operated for approximately three hours, during which the voltage, mass flow and coil current were held fixed, except for a fine tuning of the coil current in the first few minutes after turn-on. Using a Fluke Hydra data-logger, the thermocouple readings were sampled every 10 seconds. Temperature monitoring continued for more than an hour after thruster turn-off.

Fig. 2 shows the temperature profiles measured by T1-T6 during thruster operation at 600 Watts. As can be seen, the temperature at T4, the closest to the acceleration region, rises initially the fastest. However, after about 45 minutes it is surpassed by T1 and T2. This behavior may well be a result of the increased role of radiation as the temperature rises, causing external parts to reach steady-state faster than internal ones. T1 reached 95% of its steady-state value after 77 minutes and 99% after 103 minutes. After two and a half hours of operation the temperatures of all six thermocouples were already very stable, with T1-T4 fluctuating no more than ±0.1°C while the temperatures at T5 and T6 continued to rise at a slow rate of approximately 1°C/hour.

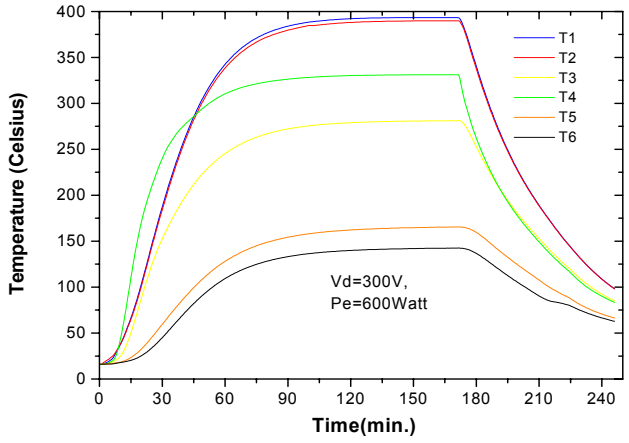

Figure 2: Temperatures versus time measured by T1-T6 during thruster operation at 600 Watts.

The temperature profiles in the two lower power cases look very similar to Figure 2 with the time to steady-state somewhat longer and the steady-state temperatures somewhat lower. At 306 Watts, T1 reached 95% of

its steady-state value after 95 minutes and 99% after 133 minutes. In the cases of coil current and no operation, more than 4 hours were needed to come close to thermal steady-state, and the temperatures indeed were much smaller. The T1-T6 steady-state temperatures for the three power level cases are presented in Table 2. The second column in Table 2 shows the total power dissipated in the coils in each case. In order to check the reproducibility of the results, The measurements at 430 and 600 Watts were repeated. A deviation of no more than 8°C in the reading of a thermocouple was observed. As can be seen from Table 2, doubling the input power leads to only a modest increase in the steady-state body temperatures. This behavior may be a result of the following factors: 1. Thruster cooling and hence the steady-state are dominated by radiation, $P_{rad} \sim T^4$; 2. The increased efficiency at the higher power; 3. The coil dissipated power is almost the same.

Table 2: Steady-state thruster body and near exit channel surface temperatures.

Thruster Power (Watts)	Coil Power (Watts)	T1 (°C)	T2 (°C)	T3 (°C)	T4 (°C)	T5 (°C)	T6 (°C)	Tex (°C)	Tin (°C)
300	21.5	349.7	347.9	249.7	290.2	148.0	125.3	-	-
430	22.7	370.7	370.4	267.6	316.6	157.5	135.4	535	576
600	22.8	393.3	389.9	281.1	331.1	165.4	142.5	570	603

Shown also in table 2 are the near exit channel surface temperatures: Tex – of the external wall, and Tin – of the internal wall. Tex and Tin were measured with an Inframetrics – 760 thermal imaging camera. The camera imagined the thruster through a Germanium window mounted on a flange facing the thruster on the side of the vacuum chamber. The attenuation of the Germanium window was calibrated by comparing the visible temperature of a variable temperature hot body with and without the window. The visible temperature was corrected also for the emissivity of the BN ceramic taken to be 0.75 [3]. In order to observe both the near exit internal and external channel walls, the thruster, normally aligned with the chamber axis, was tilted by an angle of 10°. A thermal imaging photo of the thruster channel exit during operation is depicted in Fig. 3, showing both the internal and external walls. The local temperature sampling cursor is positioned on the internal wall. Due to the limited time of availability of the camera, measurements were taken only in the 430 and 600 Watts cases.

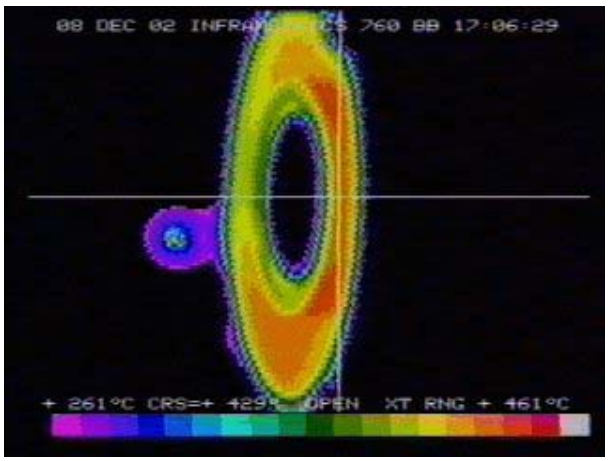

Figure 3: A thermal imaging photo of the thruster channel exit. The cursor is positioned on the internal wall.

3. Loss budget estimates

The purpose of the following analysis is to provide rough estimates for the power dissipated in the thruster internal surfaces during its operation. These estimates serves then as first iteration input to the finite element thermal model of the thruster.

The thruster efficiency can be written as [1]:

$$\eta = \eta_m \cdot \eta_v \cdot \eta_I , \tag{1}$$

where η_m is the ratio of the thrust power, $\frac{T^2}{2\dot{m}}$, to the ion jet kinetic power, $\frac{1}{2}\dot{m}_i v_i^2$, and thus does not represent proper energy losses. Here, T is the thrust, $\dot{m}$ is the thruster mass flow, while $\dot{m}_i$ and v_i are respectively the ion mass flow and average velocity at the thruster exit. The main contribution to η_m comes from the propellant utilization, and there is also some contribution from the jet divergence. The voltage utilization, η_v, and the current utilization, η_I, are defined by:

$$v_i \equiv \sqrt{\frac{2e\eta_v V_d}{m_i}}; \qquad \eta_I \equiv \frac{I_i}{I_d}, \tag{2}$$

where e and m_i are respectively the ion charge and mass, V_d and I_d are respectively the thruster discharge voltage and current, and I_i is the ion current at the thruster exit. Using Eq. (2) we can write the fraction of the thruster input electric power, $P_e = I_d V_d$, which is lost and not converted to kinetic power as:

$$P_l = (1 - \eta_I \eta_v) P_e \tag{3}$$

Ion current measurements of a small Hall thruster with a BN channel, operating at the optimal magnetic coil current point (minimum discharge current), indicated that in the voltage range of 250-400V, $\eta_I \approx 0.7$ [1]. Average ion energies of 250-260 eV, measured with SPT-100 class thrusters operating at 300V [4,5], correspond to a value of about 0.85 for the voltage utilization. This value is consistent with a thruster efficiency of 0.5 and a propellant utilization of 0.88 (cathode not included), obtained in [1] for thruster operation at 300V, relatively large mass flow and at optimal coil current, with a plume divergence cosine factor of 0.97 [6], and with the above mentioned value for the current utilization, where we have made use of Eq. (1). Using Eq. (3), we obtain then a value of $0.405P_e$ for P_l. Not all of this power is dissipated in the thruster body. The following is an estimate for the power losses outside the thruster body:

1. **Cathode losses:** The cathode assembly geometry is not included in the present version of the thruster thermal model, and so cathode losses are regarded here as external. A typical cathode voltage drop is 15V. Then, the power dissipated in the cathode is estimated to be $15 \cdot I_d = 0.05P_e$.

2. **Ionization energy:** The first ionization potential of xenon is 12.1 eV. The power lost to ionization is then estimated to be $12.1 \cdot I_i \approx 12.1 \cdot 0.7 \cdot I_d \approx 0.03 P_e$.
3. **Electron heat conduction in the plume:** A typical electron temperature in the plume is 3 eV. Hence we assume an electron enthalpy of $2.5kT_e = 7.5$ eV. Then, assuming also a quasi-neutral plume, the heat carried by the plume electrons is estimated to be $7.5 \cdot I_i \approx 7.5 \cdot 0.7 \cdot I_d \approx 0.02 P_e$.

The estimate for total power losses outside the thruster body is thus $(0.05 + 0.03 + 0.02)P_e = 0.1P_e$. From which follows that the estimate for the power dissipated inside the thruster, for operation at 300V, relatively large mass flow and optimal coil current is $0.305P_e$. At a constant voltage, the input power is decreased by reducing the mass flow. As the mass flow is reduced, so does the thruster efficiency [1]. This is attributed mainly to the drop in the propellant utilization due to a lower ionization efficiency [1]. Nevertheless, a careful observation of the results in [1] indicates that there is also some increase in proper energy losses. We can then expect that the power dissipated in the thruster body will increase above the estimate of $0.305P_e$, as the mass flow is reduced.

This power is dissipated mainly in the channel walls near the exit where most of the voltage drop occurs and, as a result, the ions and the electrons are energetic, and in the anode. Assuming a typical electron temperature of 10 eV, and therefore an electron enthalpy of 25 eV, at the anode, a rough estimate for the power dissipation there is $25 \cdot I_d \approx 0.08 P_e$ It follows then that the power dissipated at the channel walls near the exit is approximately $0.225P_e$ (or larger for a reduced mass flow).

4. Thruster thermal modeling and comparison with measurements

4.1 Model Description

A steady-state thermal model of the thruster was constructed using the 3D finite-element SRAC COSMOS/Works [7] code. The model, which takes care of heat conduction and surface radiation, enables to predict the temperature distribution in the various parts of the thruster. It consists of a sectioned symmetrical quarter of the thruster assembly, cut by two perpendicular planes of symmetry. (See Figure: 4). The model includes the geometry of the following components: a) aluminum cover; b) ceramic channel; c) channel holder; and magnetic circuit which consists of d) central and outer coils, including their magnetic cores and cylindrical foil wrapping; e) magnetic screens; f.) external magnetic pole. The present version of the model does not include the detailed geometry of the anode and cathode assemblies. Nevertheless, these parts were represented by their effective loads as described below.

In general, the thermal properties of the materials used in the model were taken from the TPRC [3]. A laboratory test was conducted to evaluate the thermal conductivity coefficient of the channel material, which was found to be 8.5 Watts/m/°C. This coefficient has a crucial effect on the ability of the heat to penetrate

from the near exit channel end towards the center of the thruster and therefore it has a great influence on the thruster temperature distribution. In addition, thermal contact resistances were considered between mechanically assembled parts. The thermal contact resistances were obtained by calibrating the thermal model results according to the measured temperatures in two cases in which there was heat dissipation only in the coils, i.e., the coils carried current but the thruster was not operated.

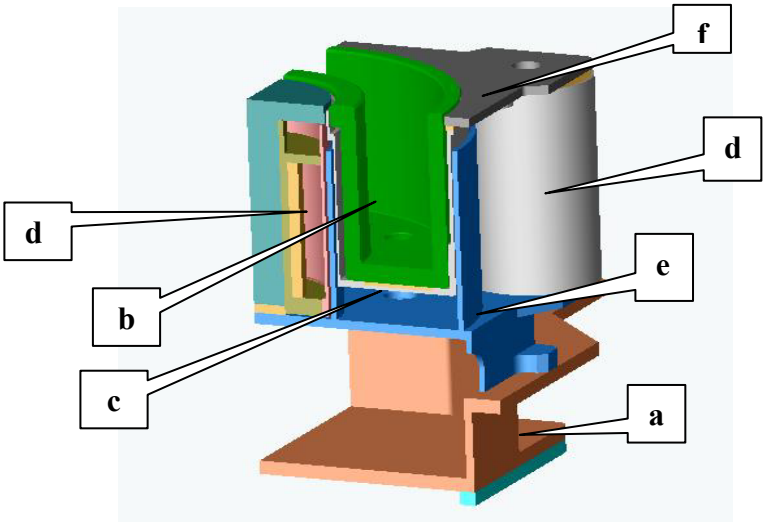

Figure: 4: The thruster thermal model and its components

4.2 Heat Losses and power Dissipation

In accordance with the discussion in section 3, heat loads were assumed on the following locations: 1. The near exit channel surfaces ("acceleration region"); 2. On the back channel surface, where the anode is mounted in the real thruster, representing the heat load on the anode ("effective anode"); 3. On the cover plate representing the heat load coming from the cathode assembly ("effective cathode"). The estimates of section 3 served as first iteration input to the thruster thermal model. In addition, The heat dissipated in the magnetic coils were evaluated using the coil's current and the wire resistance of each coil. The temperature dependent wire resistance was deduced from the manufacturer curves. Mutual surface radiation power loads and their view factors were calculated separately using basic thermal radiation relations.

Although the Cosmos/Works code treats surface radiation to background, it does not include mutual surface radiation calculations. To overcome this limitation, it was augmented by an iterative process as follows. The model was first run with the power loads mentioned above. The temperatures obtained were used then to recalculate the mutual surface radiation loads and to rerun the model until convergence was reached.

4.3 Thermal model results and comparison with measurements

Following the estimates in section 3, the main loads affecting the temperature distribution of the thruster are on the internal and external channel walls. Although we had a rough estimate for the total heat load on both of the walls (see section 3), we did not have an a-priori estimate of what portion is dissipated on each of them. It was observed in simulations that any arbitrary assumption could lead to a quite different thruster temperature distribution. In this regard, the thermal imaging camera measurements of Tex and Tin (at 430 and 600 Watts, see section 2) were very crucial. They were used to repartition the total heat loads on the channel walls until a close match to these temperatures was obtained.

The other "key temperatures" are T1 and T4, on the central coil and on the top of the channel holder. The temperature differences between T1 and T2 were always very small, in measurements as well in simulations. T5 and T6 are located on the cathode and anode assemblies, which are not included in the present version of the model, while T3 is located very close to the anode (see Fig. 1). We tried to match the T1 and T4 measurements as close as possible, by modifying the total power dissipated inside the channel. We found by this "matching procedure", that for the input thruster power level case of 600 Watts, the fraction of this power that is dissipated as heat losses inside the thruster, 30.3%, is very close to the estimate of section 3. As expected in section 3, it was found also that the heat losses fraction inside the thruster increased at the two lower input thruster power levels: For 430 Watts we got 34.9%, and for 306 Watts, we got 39.9%. It was found also by this procedure that the heat flux (the heat load divided by the surface) was greater on the internal wall than on the external one for all three power levels. The ratio between the heat fluxes was 1.21 for 600 Watts, 1.25 for 430 Watts, and 1.38 for 306 Watts (though the ratio result for 306 Watts should be regarded with more caution since thermal imaging measurements were not performed at this power level).

A summary of the thermal model results is presented below. The Heat load rates at the three thruster power levels and in the two cases in which the coils carried current but the thruster was not operated, are presented in table 3. A comparison with the measured steady-state temperatures at T1, T4, Tin and Tex is presented in table 4. As can be seen, very good matching was obtained in most cases with the maximal deviation being 7°C in one case. This deviation is comparable to the 8°C maximal deviation obtained in the repeated measurements (see section 2). The calculated heat loss fractions and heat flux ratios are also presented in table 4. Figure 5 shows the simulated steady-state thruster temperature distribution for the power level case of 600 Watts.

Table 3: Heat load rates at the three thruster power levels and in the two cases in which the coils carried current but the thruster was not operated (Ic – coil current).

Thruster power (watts)	Heat load locations and rates (Watts)					
	Internal wall	External wall	Effective Anode	Inner coil	Outer coil	Effective Cathode
306	44.59	51.72	25.75	7.78	2.76	12.60
430	50.20	64.01	36.25	7.32	3.07	13.69
600	56.50	74.8	50.5	7.97	3.03	15.14
0 (Ic=2.52A)	-	-	-	6.19	3.06	-
0 (Ic=2.25A)	-	-	-	4.58	2.26	-

Table 4: A comparison of calculated and measured steady-state temperatures and the calculated heat loss fractions and heat flux ratios (Ic – coil current).

Thruster Power (Watts)	T1 (°C)		T4 (°C)		Tin (°C)		Tex (°C)		Channel Losses (%)	Heat* flux ratio
	Tested	Cal.	Tested	Cal.	Tested	Cal.	Tested	Cal.		
306	348	348	290	290	-	546	-	486	39.9	1.38
430	371	371	316	313	583	581	538	531	34.9	1.25
600	393	394	331	338	603	603	570	569	30.3	1.21
0 (Ic=2.52A)	155	158	104	104	-	-	-	-	-	-
0 (Ic=2.25A)	142	138	91	88	-	-	-	-	-	-

*Heat flux ratio between the internal and external channel walls

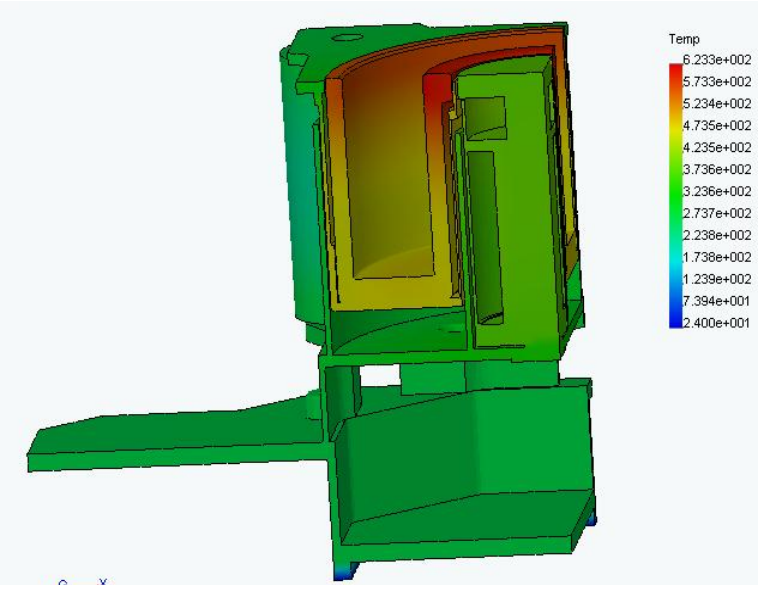

Figure: 5: Simulated steady-state thruster temperature distribution at power level of 600 Watts.

5. Summary & conclusions

Body temperatures of an engineering model Hall thruster were measured with six embedded thermocouples at three power levels. Channel surface temperatures were sampled with a thermal imaging camera.
It was observed that doubling the thruster power from 306 to 600 Watts leads to a modest increase in the steady-state body temperatures of less than 14%. It takes more than an hour for the thruster to approach a thermal steady-state, the time being longer for lower input power.

A 3D finite element thermal model of the engineering model Hall Thruster was constructed. By matching the thermal model results as close as possible to the measured steady-state temperatures at four key locations, we were able to calibrate the model. The simulation results indicate that the fraction of the input power dissipated inside the thruster increases for lower power levels, as well as the ratio of the heat fluxes between the internal and external channel surfaces. More thermal measurements and modeling, in addition to direct measurements and modeling of the plasma processes inside the channel may be needed in order to verify these interesting results.

We intend to use the calibrated thermal model as a tool that will enable to predict reliably thruster temperatures and heat loads under different operating conditions and design modifications. Future extensions of this work include thermal imaging measurements of anode temperatures, improvement of the thruster thermal model to include anode and cathode assemblies, and time-dependent simulations.

References

[1] J. Ashkenazy, Y. Raitses and G. Appelbaum, *Parametric Studies of the Hall Current Plasma Thruster*, Physics of Plasmas, **Vol. 5,** pp. 2055-2063, May 1998.

[2] J. Ashkenazy, G. Appelbaum, M. Guelman and A. Kogan, *Torque Control of Hall propelled Small Spacecraft*, IEPC-99-183, Proc. 26th Inter. Electric Propulsion Conf., Kitakyushu, Japan, Oct. 1999.

[3] Y.S.Touloukian, "Thermo Physical Properties of Matter", IFI\Plenum, NY-Washington, 1977.

[4] L. B. King and A. D. Gallimore, *Ion Energy Diagnostics in the plume of an SPT-100 from Thrust Axis to Backflow Region*, AIAA-98-3641, 34th JPC, Cleveland, July 1998.

[5] C. Perot et al., *Characterization of a Laboratory Hall Thruster with Electrical Probes and Comparisons with a 2D Hybrid PIC-MCC Model*, AIAA-99-2716, 35th JPC, Los Angeles, June 1999.

[6] V. M. Gavryushin and V. Kim, *Effect of the Characteristics of a Magnetic Field on the Parameters of an Ion Current at the Output of an Accelerator with Closed Electron Drift*, Sov. Phys. Tech. Phys., **26(4**), pp. 505-507, April 1981.

[7] COSMOS/Works 7.0 Date Code 2002/144, Structural Research & Analysis Corp.